



Research paper

Morphology and defects regulation of carbon nitride by hydrochloric acid to boost visible light absorption and photocatalytic activity



Changchang Dong^a, Zhiyuan Ma^b, Runtian Qie^a, Xuhong Guo^{a,c}, Cuihua Li^a, Rongjie Wang^a, Yulin Shi^a, Bin Dai^a, Xin Jia^{a,*}

^a School of Chemistry and Chemical Engineering/Key Laboratory for Green Processing of Chemical Engineering of Xinjiang Bingtuan, Key Laboratory of Materials-Oriented Chemical Engineering of Xinjiang Uygur Autonomous Region, Engineering Research Center of Materials-Oriented Chemical Engineering of Xinjiang Bingtuan, Shihezi University, Shihezi 832003, People's Republic of China

^b Département de Chimie, Université de Montréal, C.P. 6128, Succursale Centre-Ville, Montréal, Québec H3C 3J7, Canada

^c State Key Laboratory of Chemical Engineering, East China University of Science and Technology, Shanghai 200237, People's Republic of China

ARTICLE INFO

Article history:

Received 3 April 2017

Received in revised form 6 June 2017

Accepted 10 June 2017

Available online 12 June 2017

Keyword:

Ultrathin carbon nitride nanosheets

Visible light photocatalysis

Morphology and defect regulation

ABSTRACT

In this work, a hydrochloric acid assisted exfoliation approach to prepare the ultrathin carbon nitride (U-CN) nanosheet and to regulate its morphology and defects was reported. Based on moderate oxidation of hydrochloric acid, bulk carbon nitride (BCN) was just right broken into small pieces with protonation, which is beneficial to the exfoliation of BCN to U-CN nanosheets. Meanwhile, the main structure of CN do not be destroyed. Moreover, hydrochloric acid gives priority to cleave the bridging N atoms with rich electrons, leading to the formation of the favorable defects and improving its photocatalytic performance. The obtained U-CN nanosheets prepared in a suitable HCl concentration exhibits enhanced photocatalytic efficiency for hydrogen evolution and Rhodamine B degradation under visible light. Such U-CN nanosheets with simple preparation, low cost, good yield and good photocatalytic activity might shed light on an acid-assisted method for developing high-performance CN photocatalysts.

© 2017 Elsevier B.V. All rights reserved.

1. Introduction

With the increasingly serious global energy crisis and environmental contamination, photocatalysis technology has become a popular topic, which could address those problems via water splitting, carbon dioxide conversion, and water purification [1–7]. Titanium dioxide (TiO_2), which has promising energy and environmental applications, is the widely studied photocatalyst owing to its low cost, high stability, and excellent recyclability [7–10]. However, high recombination rate of photo-induced charge carriers and the large bandgap (3.2 eV for anatase) of TiO_2 have greatly limited its widespread applications [3,11–13]. Recently, graphitic carbon nitride ($g-C_3N_4$), a metal-free polymer, has gained considerable popularity, due to its visible-light-driven bandgap, proper band edges, and environmental benignity [14–17]. However, the photocatalytic activity of BCN synthesized by thermal condensation is poor, which make it far from practical application [18]. Many efforts have been contributed to enhancing the photocatalytic activity of BCN, including metal and metal-free element doping [19,20],

transition metal heterostructure formation [16,21–25], and nanostructure construction [26].

Recently, various nanostructures have been designed and prepared successfully, such as nanospheres [27], nanomeshes [26], and nanosheets [28]. They always have an increased specific surface area, a promoted ultrahigh charge carrier mobility and an enhanced energy band structure, which could effectively improve photocatalytic activities of CN [29,30]. CN nanosheet, the simplest and widely applied structure, have been of great interest to researchers in past few decades [26,31,32]. Niu et al. prepared the CN nanosheets by the thermal etching of BCN in static air [29]. The resultant nanosheets possess not only a large specific surface area but also an increased bandgap, an improved electron transport ability and a prolonged lifetime of charge carriers as a result of the quantum confinement effect. When the surface energy of BCN matches that of the solvent, liquid exfoliation could be used for preparing CN nanosheets [31]. Zhang et al. theoretically calculated the surface energy of $g-C_3N_4$ (115 mJ/m²), which matches well with that of water (102 mJ/m²) [33]. CN nanosheet could be obtained via water intercalation exfoliation method. However, the yield of the obtained CN nanosheets is relative low, due to great van der Waals force between the large layers of BCN. So the yield of CN nanosheets could be improved via decrease the BCN size.

* Corresponding author.

E-mail addresses: jiaxin@shzu.edu.cn, jiaxin1976@gmail.com (X. Jia).

Acid-assisted exfoliation of BCN has been a common method to prepared CN nanosheets [28,32,34]. The acid could cleave BCN into small pieces and protonate the layers [34]. The protonated BCN with smaller size not only induces electrostatic repulsion, provides better dispersion and a larger specific surface area, but also enables the adjustment of electronic band gaps and have higher ionic conductivity [19,23]. Zhou et al. propose CN layer can be cleaved by H_2SO_4 , and various CN nanostructures including CN quantum dots, nanoleaves and nanorods could be facilely prepared in different hydrolysis conditions [24]. However, H_2SO_4 and sulphate radical formed by absorption of residual SO_4^{2-} in the CN possess strong oxidation. Besides, Zhang et al. found that the ionic conductivity and photoconduction of the CN solids have been improved after HCl treatment [35]. HCl possesses moderate oxidation, which is just right cleave the layer of BCN, so HCl is considered as an ideal candidate to control the structure and photocatalysis performance of the CN. However, the preparation of the ultrathin CN nanosheet by HCl and the influence of HCl concentration to the morphology of CN have not been reported.

Herein, U-CN nanosheets with enhanced photocatalytic activity were prepared by HCl-assisted hydrothermal exfoliation of BCN. In this exfoliation process, BCN was broken into small pieces by HCl, which is conducive to water intercalates, the disturbance of van der Waals force between the layers and the formation of U-CN nanosheets. Meanwhile, HCl solution could introduce favorable defects of CN nanosheets which could boost its photocatalytic performance. Moreover, the HCl concentration is a key factor to the exfoliation of BCN, due to its influence to the morphology regulation and the formation of the favorable defects. Therefore, the U-CN nanosheets prepared in a suitable concentration exhibit enhanced photocatalytic efficiency for hydrogen evolution and Rhodamine B degradation under visible light, which might indicate an acid-assisted method for developing high-performance CN photocatalysts.

2. Experimental section

2.1. Materials

Melamine ($\text{C}_3\text{H}_6\text{N}_6$, 99.0%) was purchased from Sigma-Aldrich. Hydrochloric acid (HCl, 37%) was obtained from the Sinopharm Chemical Reagent Co., Ltd. All chemicals are of analytical grade and were used as received without further purification. Doubly distilled water was used throughout the experiments.

2.2. Synthesis of photocatalyst

The synthesis of BCN was according to a previously reported [29]. The CN nanosheets were prepared by exfoliation of BCN as followed: BCN (1 g) and HCl solution (50 mL, 6 M) were added into a 100 mL of teflon-lined stainless steel autoclave and heated to 120 °C for 4 h. After cooled to room temperature, the photocatalyst was obtained by centrifugation-dispersion-ultrasonication cycles and dried at 80 °C under vacuum overnight, which was denoted as U-CN-6. Other samples were prepared by the same method with different initial concentration of HCl (0, 3, and 9 M), and denoted as U-CN-0, U-CN-3, and U-CN-9, respectively.

2.3. Characterization

X-ray diffraction (XRD) patterns of the as-prepared samples were recorded at room temperature by a Bruker D8 Advance X-ray diffractometer. Fourier transformed infrared (FT-IR) spectroscopy were recorded by a Nicolet IS 10 FT-IR spectrometer, using the KBr wafer technique. X-ray photoelectron spectroscopy (XPS) data were obtained with an ESCA Lab220i-XL electron spectrometer

from VG Scientific using 300 W Al K α radiation. Transmission electron microscope (TEM) images of the as-prepared samples were measured by a Hitachi HT 7700 electron microscope operated at an accelerating voltage of 100 kV. The thickness of samples were measured by atomic force microscopy (AFM, Digital D3000). The UV-vis diffuse reflectance absorption spectroscopy (DRS) was recorded on a UV-vis spectrophotometer (Hitachi, UH4150) equipped with an integrated sphere attachment, and BaSO_4 was used as a reference. Photoluminescence (PL) spectroscopy of samples was measured on an F-4600 FL spectrophotometer at room temperature (excitation wavelength at $\lambda = 380 \text{ nm}$).

2.4. Photoelectrochemical measurement

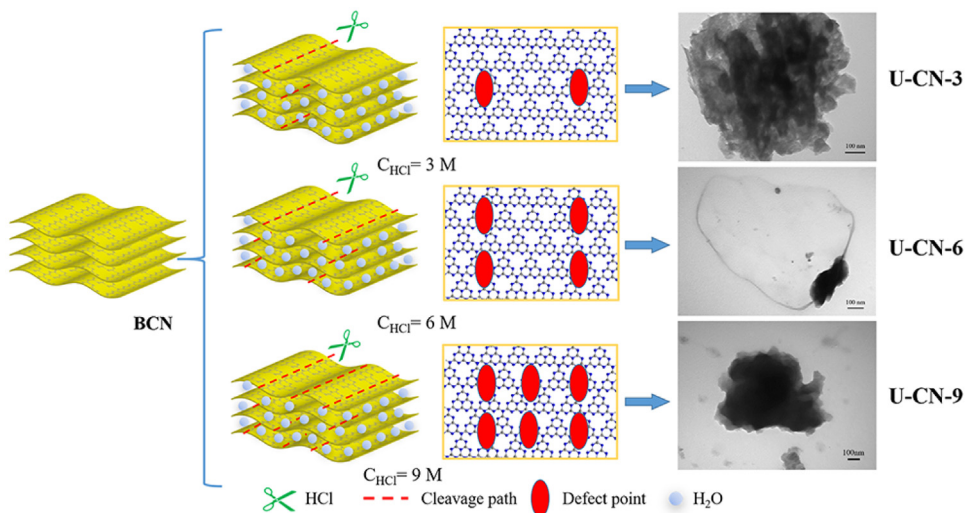
The electrochemical experiments were performed under a standard three-electrode system, with a platinum sheet used as the counter electrode, F-doped stannic oxide (FTO) glass ($1.0 \times 1.0 \text{ cm}^2$) as the working electrode and Ag/AgCl (saturated KCl solution) as the reference electrode. A bias potential of 0.5 V versus Ag/AgCl was used in the experiments, sodium sulfate solution (Na_2SO_4 , 0.1 M, pH = 7) was used as the electrolyte and a 300 W Xenon lamp (PLS-SXE 300C (BF), PerfectLight, Beijing) with an optical filter ($\lambda > 420 \text{ nm}$) was used as the visible-light source. The Mott-Schottky plots were obtained in the dark at 1000 Hz.

2.5. Photocatalytic activity

Photocatalytic hydrogen evolution reactions were recorded by a photocatalysis online analyze system (Labsolar-III, PerfectLight, Beijing). Briefly, 50 mg of photocatalysts were dispersed in 100 mL of 10 vol% triethanolamine (TEOA) aqueous solution, 3 wt% Pt was in-situ photodeposited on the surface of photocatalysts by adding H_2PtCl_6 . A 300 W Xenon lamp with an optical filter ($\lambda > 420 \text{ nm}$) was used as the visible light source. The measured average incident power of light was about 0.158 W cm^{-2} and the diameter of the light source is 6.3 cm. Before visible-light irradiation, the suspension was fully degassed to remove air. The amount of hydrogen produced was quantified by the gas chromatograph (GC D7900P, TCD detector, Ar as a carrier gas, 5 Å molecular sieve column, Shanghai Tech comp).

3. Results and discussion

U-CN nanosheets were prepared through a HCl-assisted hydrothermal exfoliation method, as showed in [Scheme 1](#). The HCl concentration is an important factor to regulate the morphology and the defects of CN. With the HCl concentration increasing, the cleavage is stronger, and more defect points are formed. But the introduction of more oxygen-containing groups lead to the stronger forces between the layers, which hinder the exfoliation of BCN. When the HCl concentration is a suitable amount, it is beneficial to the formation of CN nanosheets and the favorable defect. The crystal structures of the U-CN were characterized by XRD, as shown in [Fig. 1](#). Two obvious characteristic peaks in BCN pattern were observed at 12.6° and 27.1°, indexed as (100) and (002) peak, respectively [35]. The (100) peak can be assigned to the in-plane structural packing motif of tris-triazine units, while the (002) peak is ascribed to the interlayer stacking of aromatic segments [36,37]. However, for all U-CNs, the (100) peak becomes less pronounced, which indicates the planar size of the layers decreased during hydrothermal exfoliation of BCN [29]. The (002) peak of U-CN-0 is shifted from 27.1° to 27.3° and U-CN-3 to 9 is shifted to 27.5°, indicating a decreased gallery distance between layers [28]. Because the layers of BCN are potentially undulated, the decreased layer size caused by HCl cleavage lead to the occurrence of layer planarized [5,28]. As shown in [Fig. S1](#), the IR spectrums of all samples



Scheme 1. Schematic illustration of HCl-assisted hydrothermal exfoliation process in different concentration from BCN to CN nanosheets.

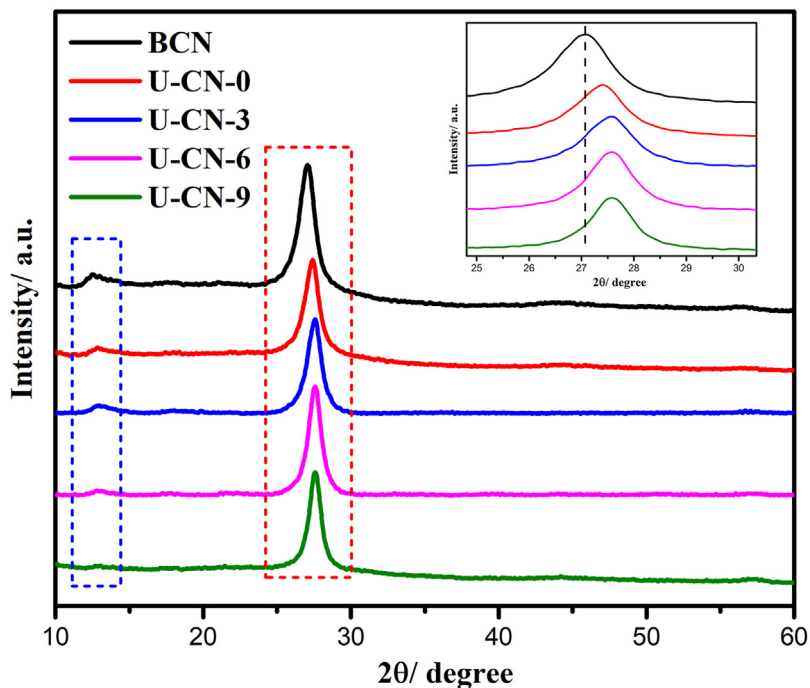


Fig. 1. XRD of BCN, U-CN-0, U-CN-3, U-CN-6, and U-CN-9.

are similar to that of BCN. The sharp peak at around 806 cm^{-1} is corresponding to the breathing mode of the triazine units. The peaks from 900 to 1800 cm^{-1} are representative of the stretching and bending modes of the C–N heterocycle. The broad peaks between 3000 and 3600 cm^{-1} are contributed by N–H stretching and surface adsorbed water molecules [16,38]. Those results indicate that the main structure of CN does not be destroyed.

The morphologies of BCN and U-CNs were investigated by TEM (Figs. 2 and S2). BCN was used as a control sample, which was prepared in the same conditions of U-CNs. For BCN, large bulk particles with obvious layer structure were observed, as shown in Fig. 2a [40]. However TEM image of U-CN-6 (Fig. 2b) shows some smaller fragments than BCN, and Fig. 2b insert shows the fragments is ultra-thin nanosheets due to the transparent rendering of TEM images. Meanwhile, the AFM images in Fig. S3 exhibit that U-CN-6 have obvious layer structure with the approximate thickness of 4.66 nm .

For U-CN-0, U-CN-3, and U-CN-9 (Fig. S2), U-CN-0 shows larger bulk particles like BCN, but the layer structure cannot be observed, due to smaller fragments of BCN have been exfoliated. U-CN-3 and U-CN-9 shows smaller particle size like U-CN-6, which indicates the cleavage have been occurred, but we cannot find an obvious ultra-thin layer structure like U-CN-6, due to the concentration of HCl is a key factor to exfoliation of BCN. When the concentration of HCl is low, the cleavage is weak, which cannot break the larger layer into small pieces. When the concentration is high, the cleavage is very strong, but the introduction of the oxygen-containing groups would lead to the enhancement of the force between the layers, which hinders exfoliation of the fragment. In both case, the exfoliation is not satisfactory. Therefore, U-CN-6 was selected in further studies.

The compositions and chemical states of BCN and U-CN-6 were studied by XPS. The full survey spectra of BCN and U-CN-6 were

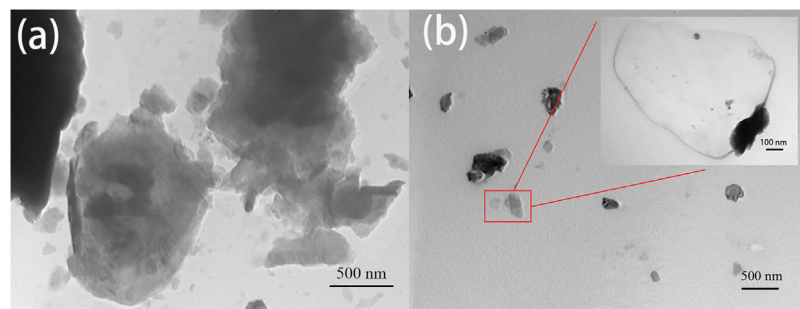


Fig. 2. TEM image of BCN (a) and U-CN-6 (b).

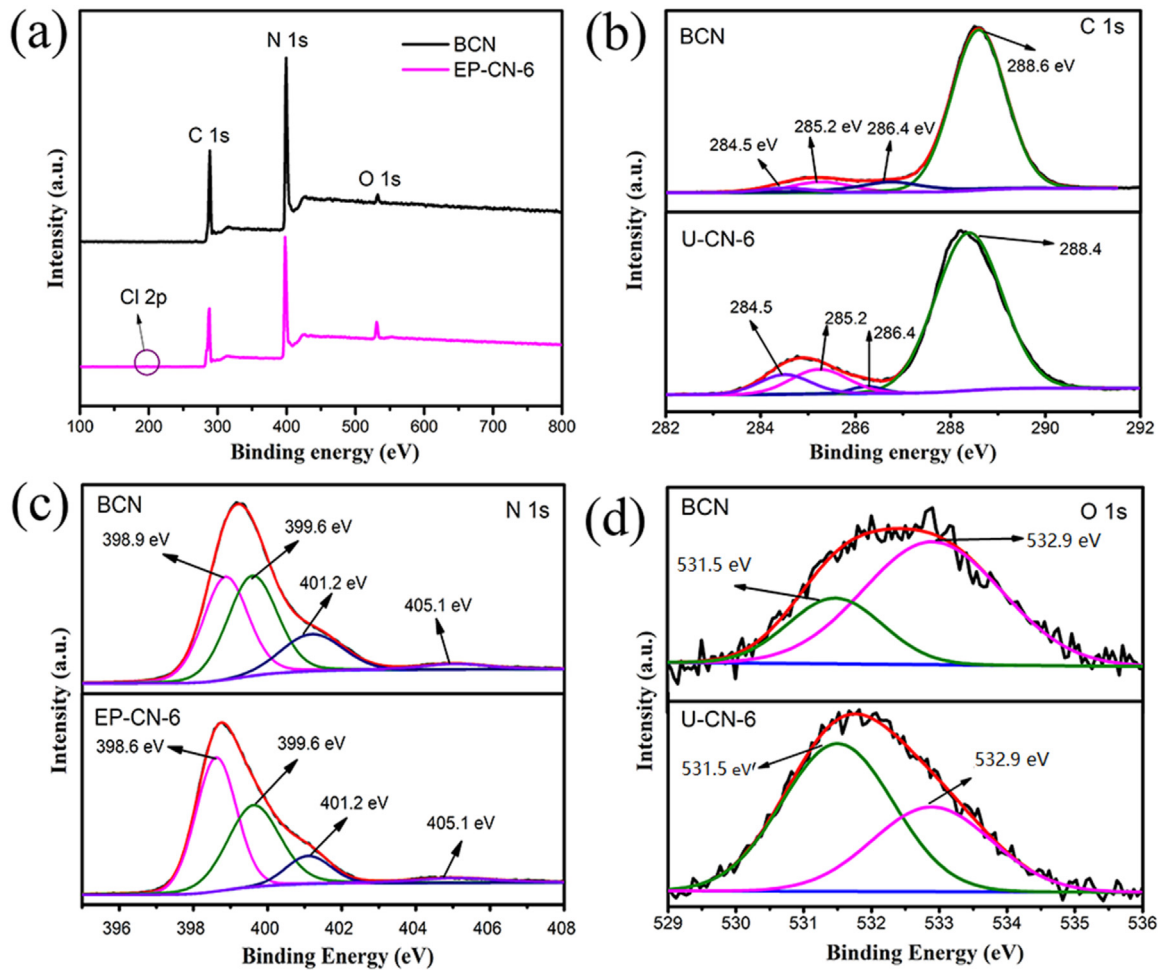
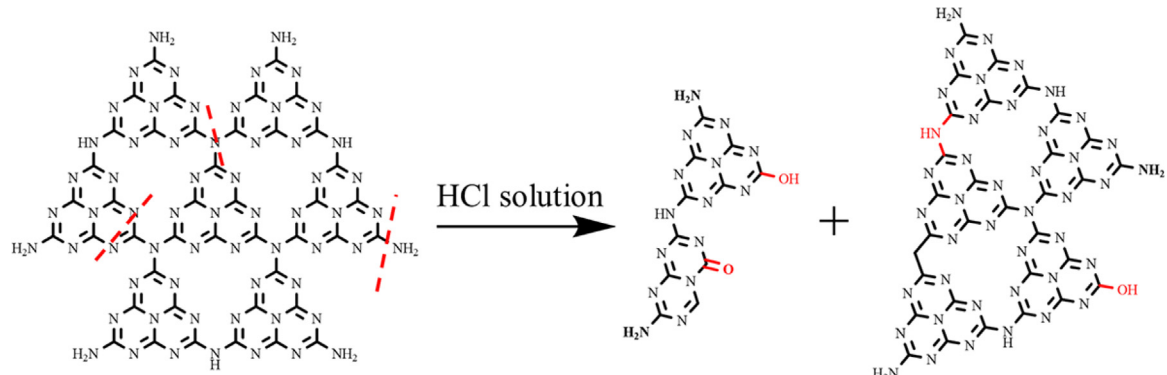


Fig. 3. XPS of BCN and U-CN-6.



Scheme 2. The possible cleavage position of BCN.

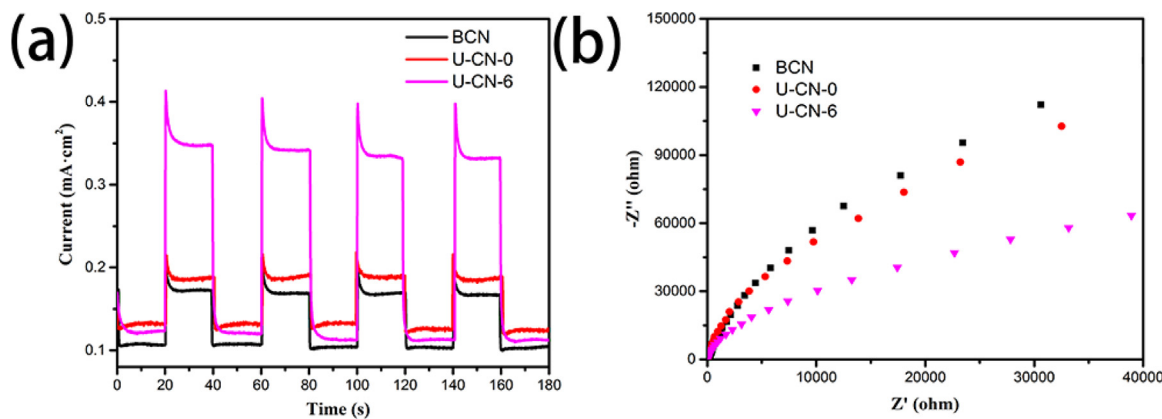


Fig. 4. Transient photocurrent responses (a) and EIS (b) of BCN, U-CN-0 and U-CN-6.

shown in Fig. 3a, both samples exist C, N and O elements. Meanwhile, the very weak signal of Cl element was observed in U-CN-6, indicating the trace chlorine is residual. However, the Cl influence can be negligible due to its trace amount [41]. The elemental composition of BCN and U-CN-6 is listed in Table S1. The C/N atomic ratio increases from 0.65 (BCN) to 0.83 (U-CN-6), which indicates the decrease of amine groups from the pristine CN in the hydrothermal process [26]. Meanwhile, U-CN-6 have higher O contents than BCN, which may be caused by breakage of the layer and increase of oxygen-containing groups [37]. The high-resolution C 1s spectra of U-CN-6 (Fig. 3b and Table S2) represents four peaks at the binding energies of 284.5, 285.2, 286.4 and 288.4 eV, respectively [26,32,42]. The binding energies of 284.5 eV is corresponding to the surface adventitious carbon which is originating from defective polymerization [28]. The binding energies of 285.2 and 286.4 eV are corresponding to C—OH and C—NH, respectively [41]. The binding energy of 288.4 eV is corresponding to the typical aromatic C=N=C coordination [43]. Compared with BCN, the proportion of C—OH increase C=N=C decrease in U-CN-6, indicating the introduction of —OH and the cleavage of carbon nitride. The proportion of C—NH is also increase, the C—NH group can be assigned to the defects, which act as the recombination sites in the photocatalytic reactions, so the decrease is beneficial to separation of photogenerated electron-holes [30,39]. The high-resolution N 1s spectra (Fig. 3c and Table S3) have four peaks, which can be ascribed to sp² N atoms involved in triazine rings (C=N=C) (398.8 eV), tertiary nitrogen (N-(C)₃) (400.1 eV), N bonded with H atoms (C—N—H) groups (401.2 eV) and charging effect in heptazine rings (405.1 eV), respectively [34]. As the deconvolution results listed in Table S3, we found that the intensity of binding energy at 398.8 eV increased and the intensity of those at 400.1 and 401.2 eV decreased, which indicates the cleavage of N-(C)₃ and the destroy of C—NH. Fig. 3d represents the O 1s peak at 531.4 and 532.6 eV, which is assigned to C—O and C=O, respectively [29]. The C=O contents obviously enhanced, which indicates the cleavage of triazine units, as shown in Table S4 [32]. Therefore, the possible cleavage positon of CN layer was shown in Scheme 2. In HCl- assisted hydrothermal process, HCl preferred to attack bridging N atoms with rich elections, which lead to the formation of more C—OH and C—NH—C [37]. Therefore, HCl can regulate the defect in BCN and optimize the aromatic π-conjugated system, which could enhance photocatalytic performance [28]. Besides, C—NH₂ and triazine units were easier attacked by HCl, leading to C—OH increase and C—NH₂ decrease, so that the defect have been modified in the hydrothermal process for the enhancement of the photocatalytic activity [32].

Transient photocurrent response and electrochemical impedance spectroscopy (EIS) were recorded by an electrochemical workstation to investigate the photoelectrochemical

properties of the samples. In Fig. 4a, all samples display obvious and reproducible photocurrent responses under visible light irradiation, which indicates good separation efficiency of the photoinduced electron-hole pairs of the photocatalysts. It is well-known that the nanosheet structure is conducive to the separation of photoinduced electron-hole pairs. Therefore, the U-CN-6 have the highest photocurrent density, which was caused by its ultrathin nanosheet structure [44]. EIS (Fig. 4b) further proved the effects of acid-assisted hydrothermal treatment to charge transfer. The arc radius of U-CN-6 is smaller than BCN, which indicates the exfoliated treatment is beneficial to the improvement of the charge transfer rate, which is consistent with photocurrent response results. Because nanosheet structure provides a more freedom for the migration of photogenerated charge carriers [45].

UV-vis diffuse reflection spectrum of the photocatalysts was shown in Fig. 5a. It is found that the absorption edge of the U-CN-6 has a blueshift, compared with that of BCN. The band gap energy (E_g) estimated from the intercept of the tangents to the Tauc plots (Fig. 4b) are 2.73 eV and 2.92 eV for BCN and U-CN-6, respectively [46]. The PL spectrum of BCN and U-CN-6 at the excitation wavelength of 380 nm is shown in Fig. 5c. The emission peak of U-CN-6 has an obvious blueshift, compared with that of BCN, which is consisted with UV-vis diffuse reflection spectra results due to a result of the quantum confinement effect [28]. The Mott-Schottky analysis was employed for the characterizations of semiconductor types as well as to determine the exact band structures of the samples. The Mott-Schottky plots of BCN and U-CN-6 display a positive slope, they are n-type semiconductor, as shown in Fig. 5d [41]. Moreover, the Mott-Schottky plots further confirm that the conduction bands of BCN and U-CN-6 are -1.391 V and -1.227 V, versus Ag/AgCl, respectively, from the intercept on the abscissa [28,40]. The potentials vs Ag/AgCl were converted to the normal hydrogen electrode (NHE) using the follow relationship:

$$V_{\text{NHE}} = V_{\text{Ag/AgCl}} + V^0_{\text{Ag/AgCl vs NHE}} \quad (1)$$

where $V^0_{\text{Ag/AgCl vs NHE}}$ is 0.197 V at 25 °C [47]. The conduction bands of BCN and U-CN-6 are -1.194 and -1.030 V, versus NHE, respectively. The valence band and conduction band have the relationship as follow:

$$E_g = E_{\text{CB}} + E_{\text{VB}} \quad (2)$$

where E_g is the bandgap energy of the semiconductor, E_{CB} is the conduction band edge potential, and E_{VB} is the valence band edge potential [48]. The calculated valence bands of BCN and U-CN-6 are 1.536 and 1.890 V, versus NHE, respectively. Therefore, the electronic band structures of BCN and U-CN-6 is shown in Fig. 6. The U-CN-6 displays higher valence band potential, which indicating have the stronger oxidizing ability.

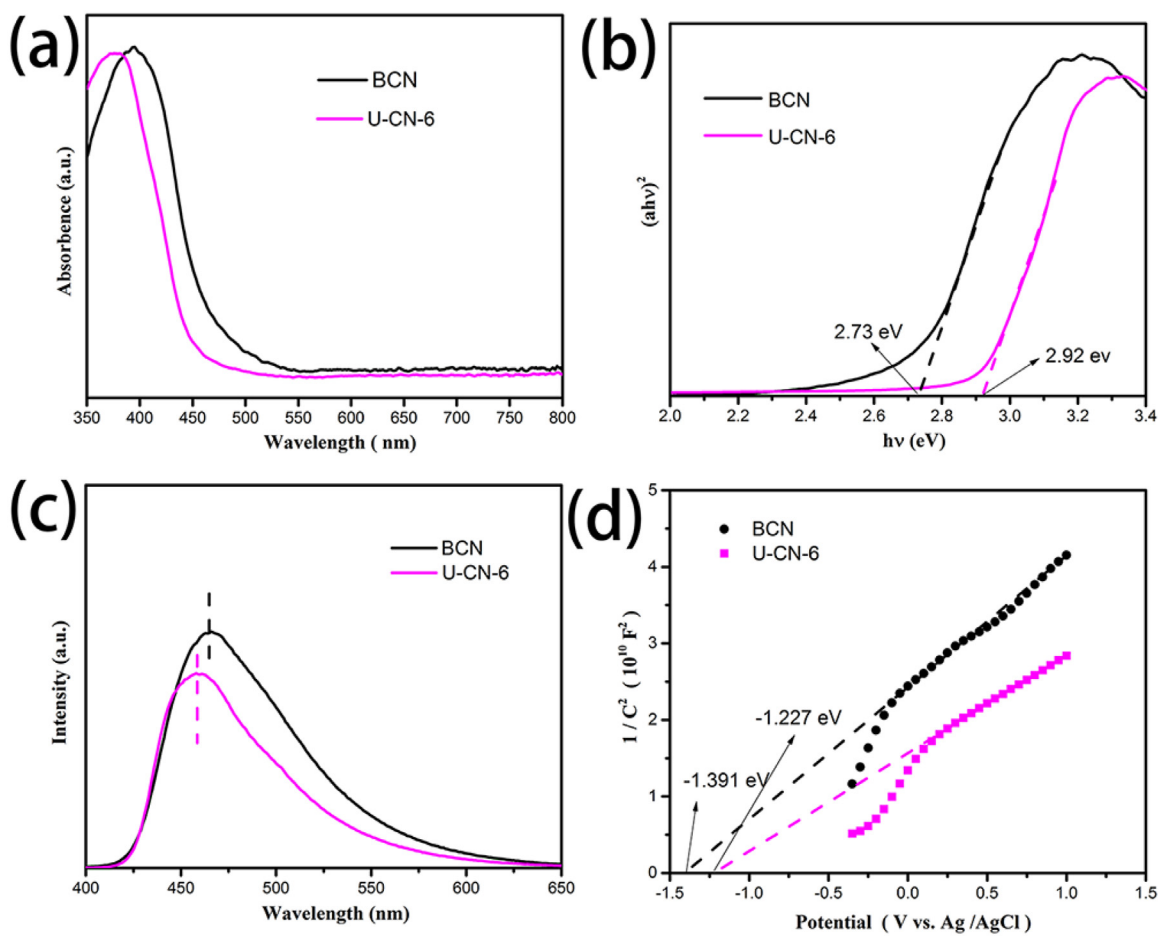


Fig. 5. DRS spectra (a), Tauc plots (b), PL spectra (c) and Mott-Schottky plot (d) of BCN and U-CN-6.

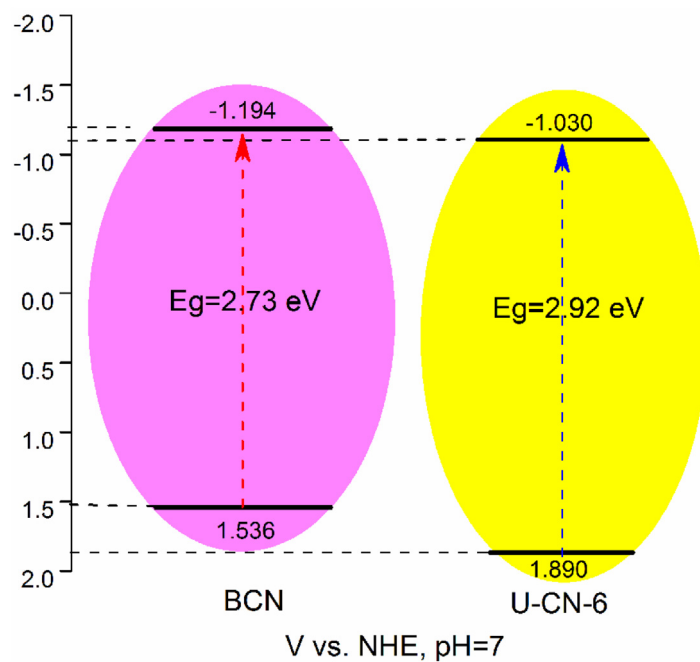


Fig. 6. Bandgap structures of BCN and U-CN-6 vs. NHE.

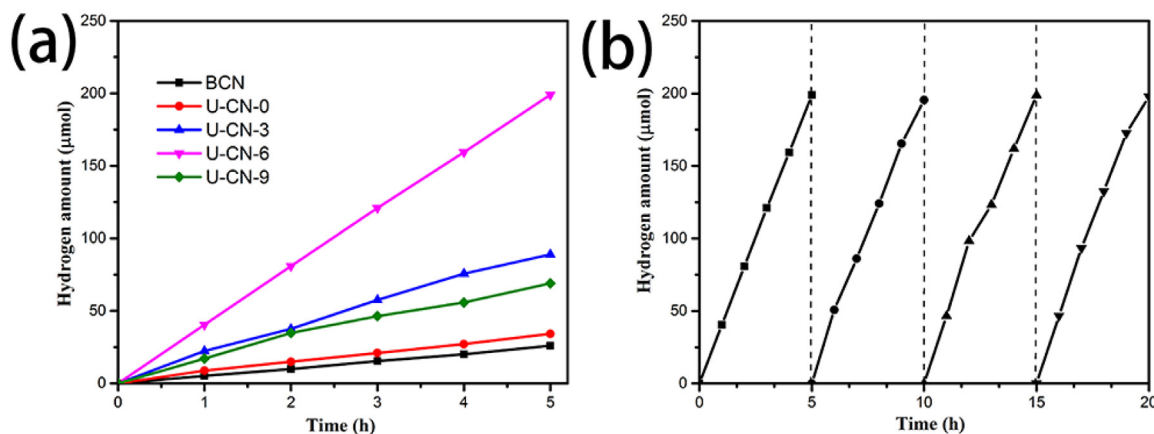


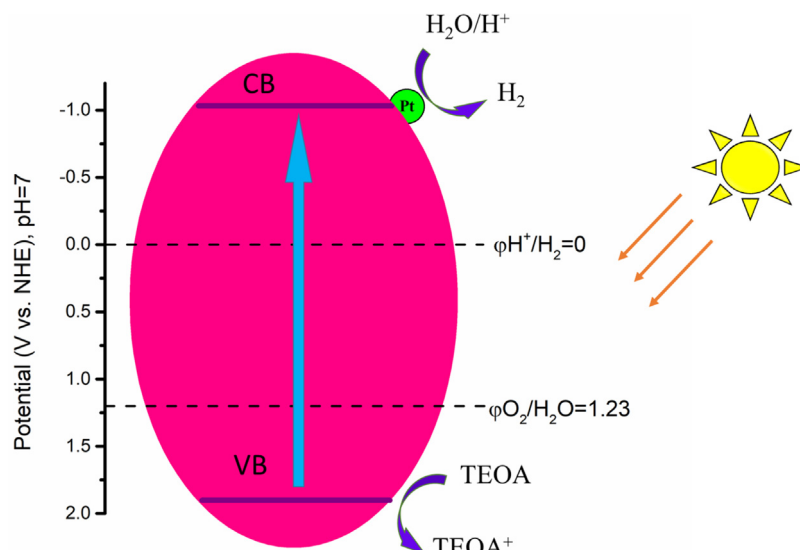
Fig. 7. (a) Photocatalytic activity for the H₂ evolution of BCN, U-CN-0, U-CN-3, U-CN-6, and U-CN-9 and (b) the photocatalytic H₂ evolution stability test on U-CN-6 under visible light ($\lambda > 420$ nm).

The photocatalytic activity of the as-prepared samples was evaluated by the photocatalytic hydrogen evolution under visible light illumination ($\lambda > 420$ nm), as shown in Fig. 6a. U-CNs exhibit the higher photocatalytic activity for H₂ evolution than BCN. After HCl treatment, the photocatalytic activity is obviously enhanced, because of the introduction of favourable defect. Among these photocatalysts, U-CN-6 shows the highest H₂ evolution rate, reaching a kinetic rate of $40.6 \mu\text{mol h}^{-1}$, which is about 7.8 times than BCN ($5.1 \mu\text{mol h}^{-1}$). The photocatalytic activity stability of U-CN-6 was evaluated by recycling the photocatalyst towards hydrogen evolution (Fig. 7b). Within 20 h, the H₂ production rates remained highly stable after 4 cycles. Meanwhile, the degradation of dye rhodamine B by as-prepared products was also studied (Fig. S4). After HCl treatment, the degradation rate enhanced obviously, and the U-CN-6 exhibits the fastest photodegradation rate. Above all, HCl not only exfoliates BCN into nanosheets, but also helps to the formation of the favourable defect, which is beneficial to the enhancement of the photocatalytic activity via the exposure of more activity sites and the decrease of recombination sites. Therefore, the U-CN nanosheets with simple preparation, low cost and good photocatalysis activity might shed light on acid-assisted method for developing high-performance CN photocatalysts.

The photocatalytic hydrogen evolution mechanism of U-CN-6 deposited by Pt under visible light illumination is showed in Scheme 3. At first, the electrons in the valence band (VB) of U-CN-6 nanosheets were excited to its conduction band (CB) under irradiation, forming the electron-hole pairs. The electrons in CB finally transferred to Pt for protons reduction product hydrogen. The generated holes in VB were captured by TEOA, which further promote the separation of electron-hole pairs. Obviously, the nanosheets structure not only provide more active sites but also reduced recombination rate of photoinduced the electron-hole pairs, further improved photocatalytic efficiency.

4. Conclusion

In this work, ultrathin CN nanosheets were successfully synthesized by a HCl-assisted hydrothermal exfoliation method. The CN layers were broken into small pieces by moderate oxidation of HCl, which is beneficial to exfoliation of BCN. Cleavage process give priority to occur in the bridging N atoms with rich elections, leading to the formation of the favorable defects. With the help of ultrathin nanosheets structure and favor defects, the obtain photocatalysts not only have improved separation efficiency of photogenerated



Scheme 3. Photocatalytic mechanism for the H₂ evolution over Pt@U-CN-6 under visible-light irradiation.

electron-hole pairs but also have enhanced photocatalytic performance. In conclusion, the HCl concentration is important factor to the exfoliation of BCN, and it also offered a guidance to acid-assisted method for developing high-performance CN photocatalysts.

Acknowledgments

This work was supported by the Natural Science Foundation of China (21364010, 51663021), Bingtuan Excellent Young Scholars (CZ027205), the Bingtuan Innovation Team in Key Areas (2015BD003) and Yangtze River scholar research project of Shihezi University (No. CJXZ201401).

Appendix A. Supplementary data

Supplementary data associated with this article can be found, in the online version, at <http://dx.doi.org/10.1016/j.apcatb.2017.06.028>.

References

- [1] K. Maeda, ACS Catal. 3 (2013) 1486–1503.
- [2] G. Zhang, Z.-A. Lan, L. Lin, S. Lin, X. Wang, Chem. Sci. 7 (2016) 3062–3066.
- [3] X. Chen, J. Wei, R. Hou, Y. Liang, Z. Xie, Y. Zhu, X. Zhang, H. Wang, Appl. Catal. B: Environ. 188 (2016) 342–350.
- [4] X. Zhao, Z. Cai, T. Wang, S.E. O'Reilly, W. Liu, D. Zhao, Appl. Catal. B: Environ. 187 (2016) 134–143.
- [5] S. Zhang, J. Li, X. Wang, Y. Huang, M. Zeng, J. Xu, ACS Appl. Mater. Interfaces 6 (2014) 22116–22125.
- [6] M.V. Sharma, V.D. Kumari, M. Subrahmanyam, J. Hazard. Mater. 175 (2010) 1101–1105.
- [7] M.V. Phanikrishna Sharma, G. Sadanandam, A. Ratnamala, V. Durga Kumari, M. Subrahmanyam, J. Hazard. Mater. 171 (2009) 626–633.
- [8] H. Yao, W. Fu, L. Liu, X. Li, D. Ding, P. Su, S. Feng, H. Yang, J. Alloys Compd. 680 (2016) 206–211.
- [9] X. Pan, X. Chen, Z. Yi, ACS Appl. Mater. Interfaces 8 (2016) 10104–10108.
- [10] T.-D. Nguyen-Phan, S. Luo, D. Vovchok, J. Llorca, J. Graciani, J.F. Sanz, S. Sallis, W. Xu, J. Bai, L.F.J. Piper, D.E. Polyansky, E. Fujita, S.D. Senanayake, D.J. Stacciola, J.A. Rodriguez, ACS Catal. 6 (2016) 407–417.
- [11] A.K.P.D. Savio, J. Fletcher, K. Smith, R. Iyer, J.M. Bao, F.C. Robles Hernández, Appl. Catal. B: Environ. 82 (2016) 449–455.
- [12] G. Williams, B. Seger, P.V. Kamat, ACS Nano 2 (2008) 1487–1491.
- [13] X.W. Lou, L.A. Archer, Adv. Mater. 20 (2008) 1853–1858.
- [14] W.J. Ong, L.L. Tan, Y.H. Ng, S.T. Yong, S.P. Chai, Chem. Rev. 116 (2016) 7159–7329.
- [15] S. Ma, S. Zhan, Y. Jia, Q. Shi, Q. Zhou, Appl. Catal. B: Environ. 186 (2016) 77–87.
- [16] Q. Liu, Y. Guo, Z. Chen, Z. Zhang, X. Fang, Appl. Catal. B: Environ. 183 (2016) 231–241.
- [17] L. Liu, Y. Qi, J. Lu, S. Lin, W. An, Y. Liang, W. Cui, Appl. Catal. B: Environ. 183 (2016) 133–141.
- [18] S. Zhang, J. Li, M. Zeng, G. Zhao, J. Xu, W. Hu, X. Wang, ACS Appl. Mater. Interfaces 5 (2013) 12735–12743.
- [19] O. Fontelles-Carceller, M.J. Munoz-Batista, M. Fernandez-Garcia, A. Kubacka, ACS Appl. Mater. Interfaces 8 (2016) 2617–2627.
- [20] S. Cao, J. Low, J. Yu, M. Jaroniec, Adv. Mater. 27 (2015) 2150–2176.
- [21] R. Hao, G. Wang, H. Tang, L. Sun, C. Xu, D. Han, Appl. Catal. B: Environ. 187 (2016) 47–58.
- [22] H. Wang, X. Yuan, H. Wang, X. Chen, Z. Wu, L. Jiang, W. Xiong, G. Zeng, Appl. Catal. B: Environ. 193 (2016) 36–46.
- [23] H. Wang, X. Yuan, Y. Wu, G. Zeng, X. Chen, L. Leng, H. Li, Appl. Catal. B: Environ. 174–175 (2015) 445–454.
- [24] Y. Liu, X. Yuan, H. Wang, X. Chen, S. Gu, Q. Jiang, Z. Wu, L. Jiang, Y. Wu, G. Zeng, Catal. Commun. 70 (2015) 17–20.
- [25] H. Wang, X. Yuan, H. Wang, X. Chen, Z. Wu, L. Jiang, W. Xiong, Y. Zhang, G. Zeng, RSC Adv. 5 (2015) 95643–95648.
- [26] Q. Han, B. Wang, J. Gao, Z. Cheng, Y. Zhao, Z. Zhang, L. Qu, ACS Nano 10 (2016) 2745–2751.
- [27] J. Sun, J. Zhang, M. Zhang, M. Antonietti, X. Fu, X. Wang, Nat. Commun. (2012) 1139.
- [28] L. Shi, K. Chang, H. Zhang, X. Hai, L. Yang, T. Wang, J. Ye, Small 12 (2016) 4431–4439.
- [29] P. Niu, L. Zhang, G. Liu, H.-M. Cheng, Adv. Funct. Mater. 22 (2012) 4763–4770.
- [30] P. Wu, J. Wang, J. Zhao, L. Guo, F.E. Osterloh, J. Mater. Chem. A 2 (2014) 20338–20344.
- [31] S. Yang, Y. Gong, J. Zhang, L. Zhan, L. Ma, Z. Fang, R. Vajtai, X. Wang, P.M. Ajayan, Adv. Mater. 25 (2013) 2452–2456.
- [32] Z. Zhou, Y. Shen, Y. Li, A. Liu, S. Liu, Y. Zhang, ACS Nano 9 (2015) 12480–12487.
- [33] X. Zhang, X. Xie, H. Wang, J. Zhang, B. Pan, Y. Xie, J. Am. Chem. Soc. 135 (2013) 18–21.
- [34] T.Y. Ma, Y. Tang, S. Dai, S.Z. Qiao, Small 10 (2014) 2382–2389.
- [35] Y. Zhang, A. Thomas, M. Antonietti, X. Wang, J. Am. Chem. Soc. 131 (2009) 50–51.
- [36] X. Liu, X. Wu, Z. Long, C. Zhang, Y. Ma, X. Hao, H. Zhang, C. Pan, J. Agric. Food Chem. 63 (2015) 4754–4760.
- [37] Y. Zeng, C. Liu, L. Wang, S. Zhang, Y. Ding, Y. Xu, Y. Liu, S. Luo, J. Mater. Chem. A 4 (2016) 19003–19010.
- [38] D.J. Martin, K. Qiu, S.A. Shevlin, A.D. Handoko, X. Chen, Z. Guo, J. Tang, Angew. Chem. Int. Ed. Engl. 53 (2014) 9240–9245.
- [39] J. Xu, Y. Li, S. Peng, G. Lu, S. Li, Phys. Chem. Chem. Phys. 15 (2013) 7657–7665.
- [40] F. Guo, J. Chen, M. Zhang, B. Gao, B. Lin, Y. Chen, J. Mater. Chem. A 4 (2016) 10806–10809.
- [41] C. Ye, J.-X. Li, Z.-J. Li, X.-B. Li, X.-B. Fan, L.-P. Zhang, B. Chen, C.-H. Tung, L.-Z. Wu, ACS Catal. 5 (2015) 6973–6979.
- [42] J. Liu, H. Wang, Z.P. Chen, H. Moehwald, S. Fiechter, R. van de Krol, L. Wen, L. Jiang, M. Antonietti, Adv. Mater. 27 (2015) 712–718.
- [43] J. Ma, C. Wang, H. He, Appl. Catal. B: Environ. 184 (2016) 28–34.
- [44] Y. Zheng, J. Liu, J. Liang, M. Jaroniec, S.Z. Qiao, Energy Environ. Sci. 5 (2012) 6717–6731.
- [45] W. Wan, S. Yu, F. Dong, Q. Zhang, Y. Zhou, J. Mater. Chem. A 4 (2016) 7823–7829.
- [46] Z.G. Liu, J.Y. Wan, Z. Yang, S.Q. Wang, H.X. Wang, Chem. Asian J. 11 (2016) 1887–1891.
- [47] F.F. Abdi, R. van de Krol, J. Phys. Chem. C 116 (2012) 9398–9404.
- [48] Y. Chen, W. Huang, D. He, Y. Situ, H. Huang, ACS Appl. Mater. Interfaces 6 (2014) 14405–14414.